Electronic Supplementary Material (ESI) for New Journal of Chemistry.
This journal is © The Royal Society of Chemistry and the Centre National de la Recherche Scientifique 2018

Electronic Supplementary Information

Nanoscale Zeolitic Imidazole Framework-90: Selective, Sensitive and Dual-excitation Ratiometric Fluorescent Detection of Hazardous Cr(VI) Anions in Aqueous Media

Hong-Guang Jin, Weibang Zong, Lin Yuan,* Xiao-Bing Zhang*

State Key Laboratory of Chemo/Biosensing and Chemometrics, College of Chemistry and Chemical Engineering, Hunan University, Changsha 410082 (PR China)

*Correspondence: xbzhang@hnu.edu.cn; lyuan@hnu.edu.cn;

Contents

Figure S1. Infrared spectra of HIca and NZIF-90.

Figure S2. High-resolution transmission electron microscope (TEM) image of NZIF-90.

Figure S3. Fluorescence spectroscopic titration of NZIF-90 water suspension with gradual addition of CrO_4^{2-} and $Cr_2O_7^{2-}$ anions (histograms).

Table S1. Performance comparisons of NZIF-90 with various MOF fluorescent sensors reported for Cr(VI) anions.

Figure S4. Fluorescence responses of NZIF-90 to different anions (240 μM) and changes in the emission with subsequent addition of equivalent amount (240 μM) of CrO_4^{2-} and $Cr_2O_7^{2-}$ anions.

Figure S5. Fluorescence spectroscopic titration of NZIF-90 water suspension with gradual addition of Fe^{3+} cation.

Figure S6. Fluorescence changes of NZIF-90 water suspension with addition of 240 μM CrO_4^{2-}, $Cr_2O_7^{2-}$, Fe^{3+} and the quenching efficiency comparisons of CrO_4^{2-}, $Cr_2O_7^{2-}$ and Fe^{3+} to the fluorescence of NZIF-90.

Figure S7. Powder X-ray diffraction (PXRD) patterns of NZIF-90 after three cycles of sensing CrO_4^{2-} and $Cr_2O_7^{2-}$ anions.

Figure S8. Fluorescence sensing of NZIF-90 to CrO_4^{2-} and $Cr_2O_7^{2-}$ anions for three cycles

Figure S9. Powder X-ray diffraction patterns (PXRD) of NZIF-90 after immersed in 3 mM $CrO_4^{2-}/Cr_2O_7^{2-}$ aqueous solution for 3 hours.

Figure S10. UV-Vis absorption spectra of various ions in the water solution.

Figure S11. Fluorescence intensity versus concentration of $CrO_4^{2-}/Cr_2O_7^{2-}$ anion at low concentration range.

Figure S12. UV-Vis absorption of RhB in water.

Figure S13. UV-Vis absorption and fluorescence emission (excitation at 373 nm) of RhB@NZIF-90 in water prepared from different molar ratios of HIca to RhB.

Figure S14. FT-IR spectra of NZI-90, RhB and RhB@NZIF-90 prepared from different molar ratios of HIca to RhB.

Figure S15. SEM images of RhB@NZIF-90 prepared from different molar ratios of HIca to RhB.

Figure S16. Fluorescence emission spectra of RhB@NZIF-90 in water after 12, 24 h standing.

Figure S17. Fluorescence excitation responses of RhB@NZIF-90 to different anions (480 μM) and changes in the excitation with subsequent addition of equivalent amount (480 μM) of CrO_4^{2-} and $Cr_2O_7^{2-}$ anions.

Figure 18. Fluorescence spectroscopic titration of RhB@NZIF-90 water suspension with gradual addition of CrO_4^{2-} and $Cr_2O_7^{2-}$ anions.

Figure 19. Fluorescence sensing experiment of NZIF-90 for CrO_4^{2-} and $Cr_2O_7^{2-}$ anions in ethanol.

Figure 20. Fluorescence sensing experiment of NZIF-90 for CrO_4^{2-} and $Cr_2O_7^{2-}$ anions in DMF.

Figure 21. PXRD patterns and SEM images of the as-synthesized μm scaled ZIF-90 and RhB@ZIF-90.

Figure 22. Fluorescence sensing experiment of μm scaled ZIF-90 for CrO_4^{2-} and $Cr_2O_7^{2-}$ anions in water.

Figure 23. Fluorescence excitation responses of μm scaled RhB@ZIF-90 to CrO_4^{2-} and $Cr_2O_7^{2-}$ anions in water.

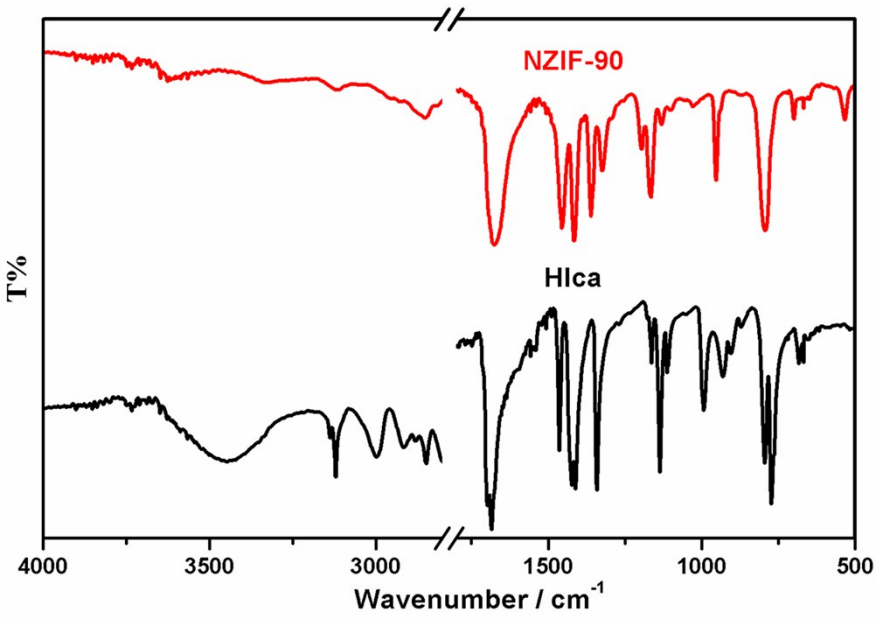

Figure S1. Infrared spectra of HIca and NZIF-90.

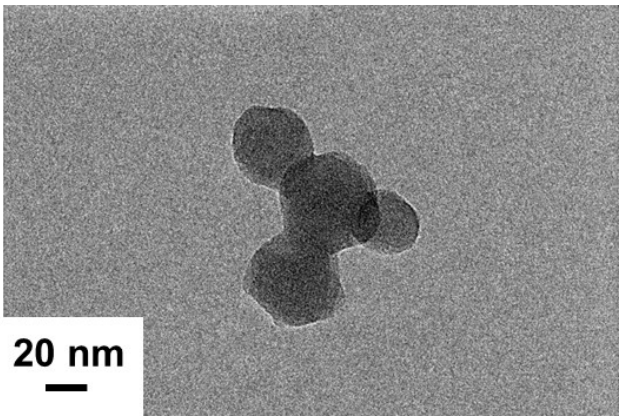

Figure S2. High-resolution transmission electron microscope (TEM) image of NZIF-90.

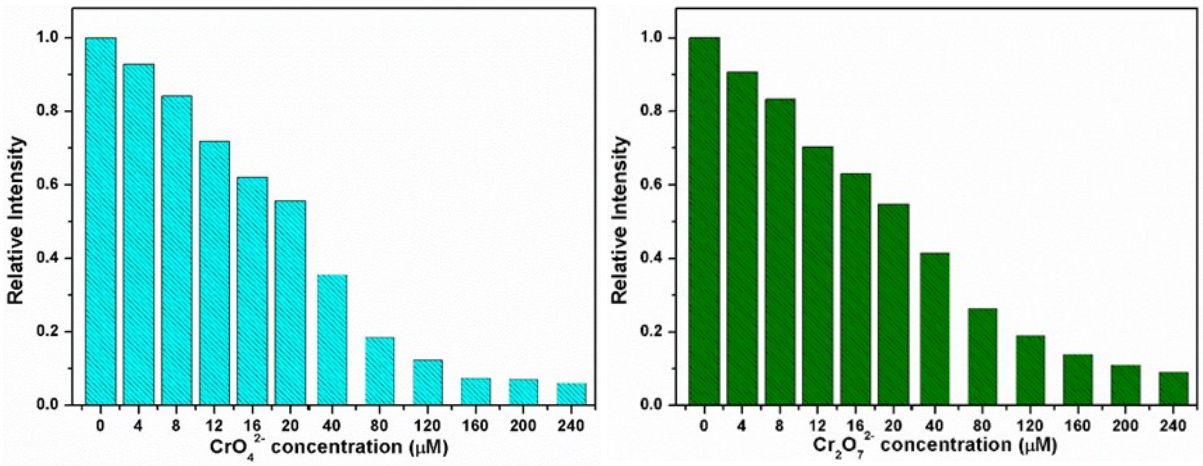

Figure S3. Fluorescence spectroscopic titration of NZIF-90 water suspension with gradual addition of CrO_4^{2-} (left) and $Cr_2O_7^{2-}$ (right) (histograms).

Table S1. Performance comparisons of NZIF-90 with various MOF fluorescent sensors reported for Cr(VI) anions.

MOF-based Probes	Analyte	Quenching Constant (K_{sv}, M^{-1})	Detection of Limit (μm)	Reference
Zn-MOF	CrO_4^{2-} /$Cr_2O_7^{2-}$	7.81×10^3/ 9.21×10^3	2.50/2.35	*Inorg. Chem.* **2017**, 56, 12348-12356
Eu^{3+}@Zn-MOF	CrO_4^{2-} /$Cr_2O_7^{2-}$	3.25×10^3/ 7.08×10^3	4.50/2.82	*Inorg. Chem.* **2017**, 56, 12348-12356
$[Zn(btz)]_n$	CrO_4^{2-} /$Cr_2O_7^{2-}$	3.19×10^3/ 4.23×10^3	10/2	*CrystEngComm* **2016**, 18, 4445-4451
$[Zn_2(ttz)H_2O]_n$	CrO_4^{2-} /$Cr_2O_7^{2-}$	2.35×10^3/ 2.19×10^3	20/20	*CrystEngComm* **2016**, 18, 4445-4451
$[Eu(Hpzbc)_2(NO_3)]\cdot H_2O$	$Cr_2O_7^{2-}$		22	*Inorg. Chem.* **2016**, 55, 3952-3959
Zn(ATA)(L)	CrO_4^{2-} /$Cr_2O_7^{2-}$	1.485×10^3/ 2.623×10^3	0.25/0.43	*Inorg.Chem.* **2017**, 56, 10939-10949
Cd(ATA)(L)	CrO_4^{2-} /$Cr_2O_7^{2-}$	0.97×10^3/ 3.119×10^3/	0.18/0.19	*Inorg.Chem.* **2017**, 56, 10939-10949
Zn(IPA)(L)	CrO_4^{2-} /$Cr_2O_7^{2-}$	1.00×10^3/ 1.37×10^3	18.33/12.02	*Inorg.Chem.* **2017**, 56, 2627-2638
Cd(IPA)(L)	CrO_4^{2-} /$Cr_2O_7^{2-}$	1.30×10^3/ 2.91×10^3	2.52/2.26	*Inorg.Chem.* **2017**, 56, 2627-2638
NUM-5	CrO_4^{2-} /$Cr_2O_7^{2-}$	1.24×10^5/ 9.40×10^4	2.58/3.24	*Chem. Eur. J.* **2018**, 24, 3192
NZIF-90	CrO_4^{2-} /$Cr_2O_7^{2-}$	6.50×10^4/ 4.00×10^4	1.41/1.78	This work

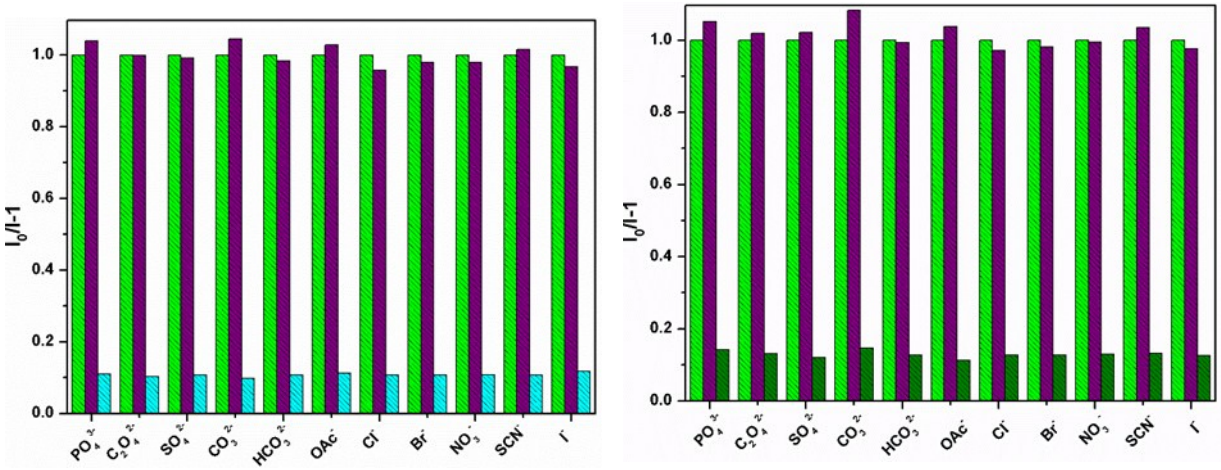

Figure S4. Fluorescence responses of NZIF-90 (green bars) to different anions (240 μM, pink bars) and changes in the emission with subsequent addition of equivalent amount (240 μM) of CrO_4^{2-} (cyan bars) and $Cr_2O_7^{2-}$ (olive bars) anions.

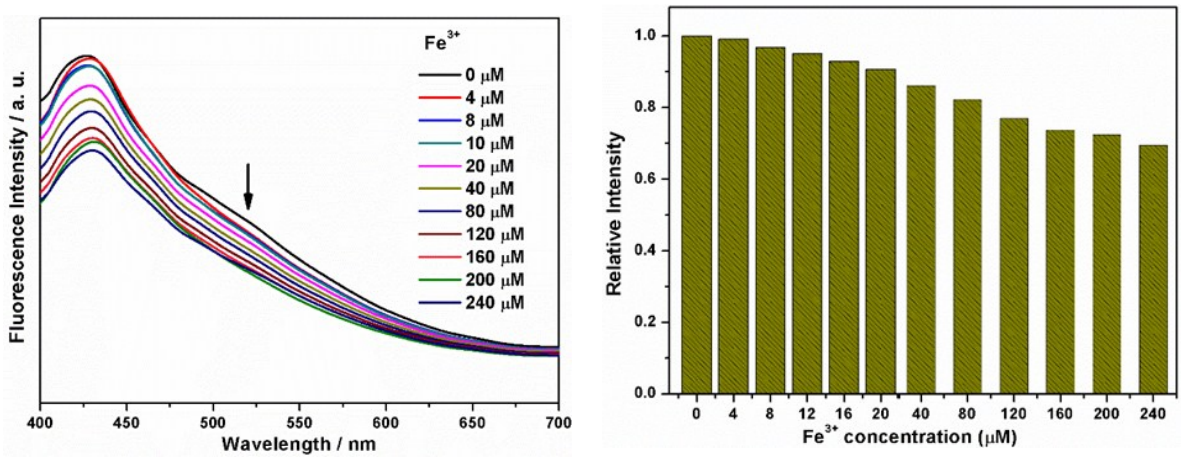

Figure S5. Fluorescence spectroscopic titration of NZIF-90 water suspension with gradual addition of Fe^{3+}cation.

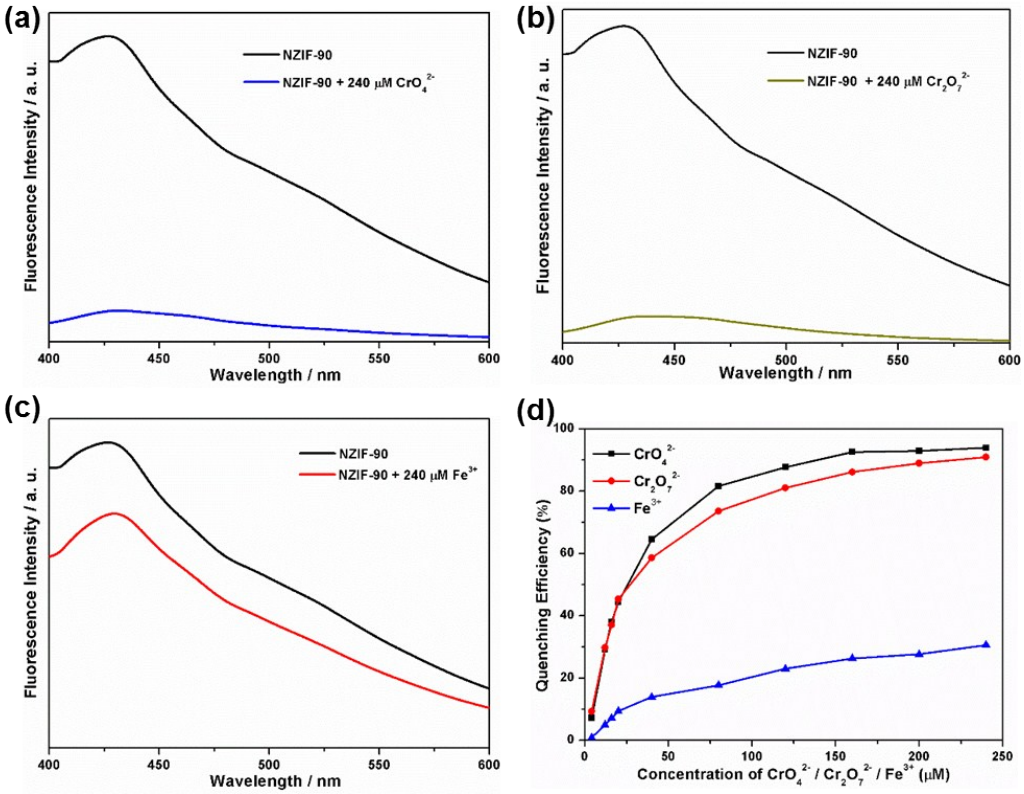

Figure S6. Fluorescence changes of NZIF-90 water suspension with addition of 240 μM CrO_4^{2-} (a), $Cr_2O_7^{2-}$ (b), Fe^{3+} (c) and quenching efficiency comparisons of CrO_4^{2-}, $Cr_2O_7^{2-}$ and Fe^{3+} to the fluorescence of NZIF-90 (d).

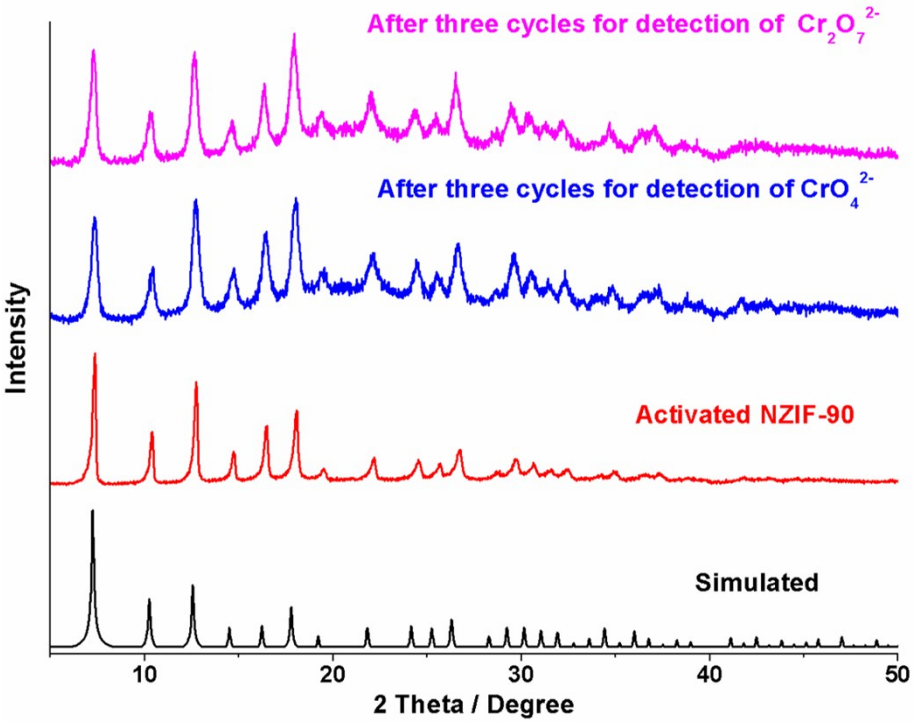

Figure S7. Powder X-ray diffraction (PXRD) patterns of NZIF-90 after three cycles of sensing CrO_4^{2-} and $Cr_2O_7^{2-}$ anions.

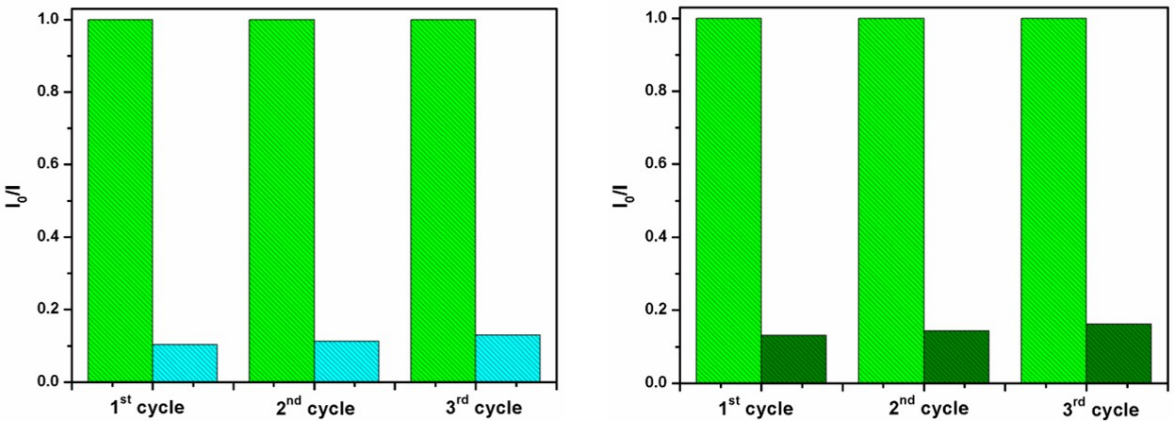

Figure S8. Fluorescence sensing of NZIF-90 to CrO_4^{2-} and $Cr_2O_7^{2-}$ anions for three cycles (green bars, the fluorescence intensity of NZIF-90; cyan bars and olive bars are the fluorescence intensities after addition of 240 μM CrO_4^{2-} and $Cr_2O_7^{2-}$, respectively).

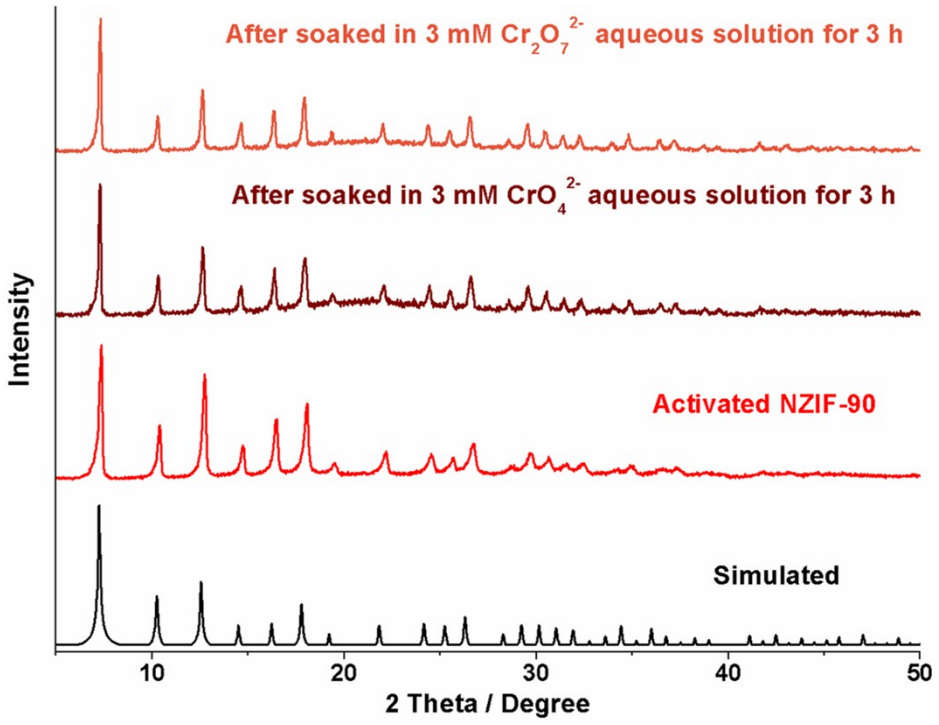

Figure S9. Powder X-ray diffraction patterns (PXRD) of NZIF-90 after immersed in 3 mM CrO_4^{2-}/$Cr_2O_7^{2-}$ aqueous solution for 3 hours.

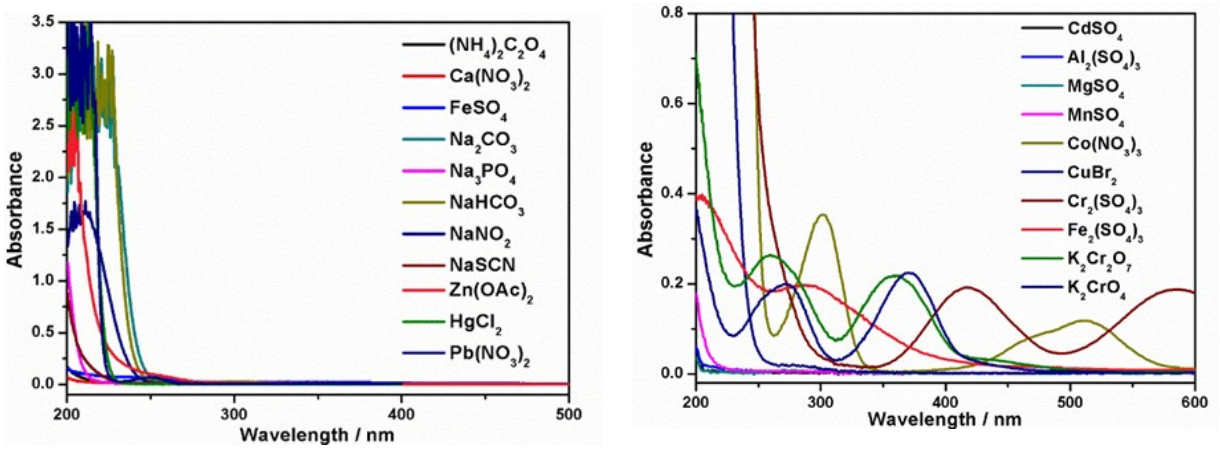

Figure S10. UV-Vis absorption spectra of various ions in the water solution.

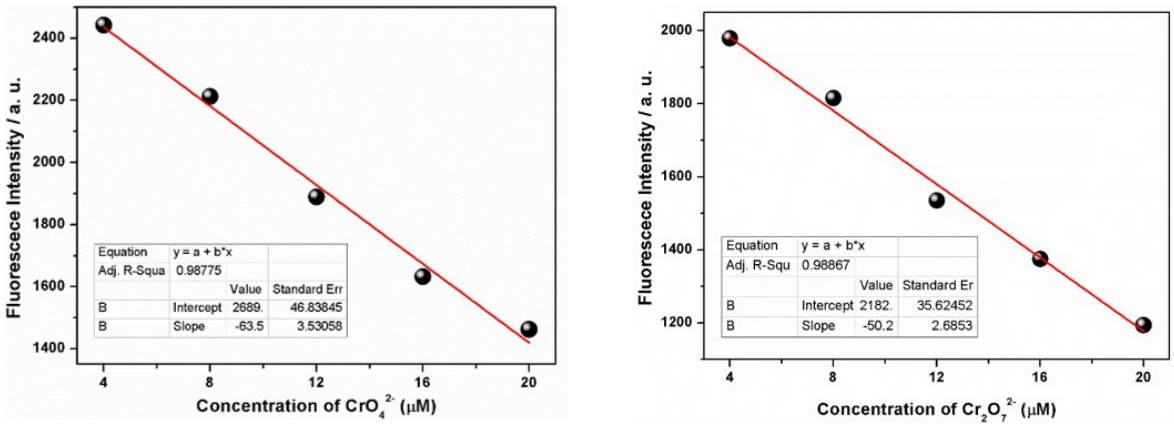

Figure S11. Fluorescence intensity versus concentration of CrO_4^{2-}/$Cr_2O_7^{2-}$ anion at low concentration range.

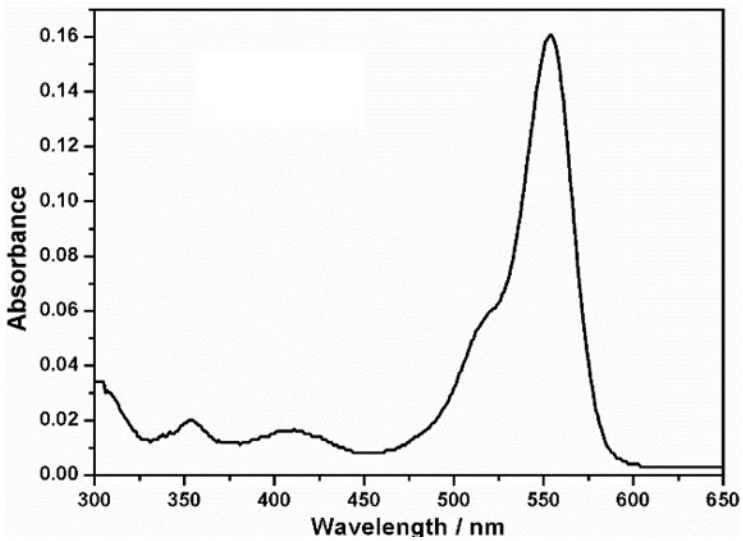

Figure S12. UV-Vis absorption of RhB in water.

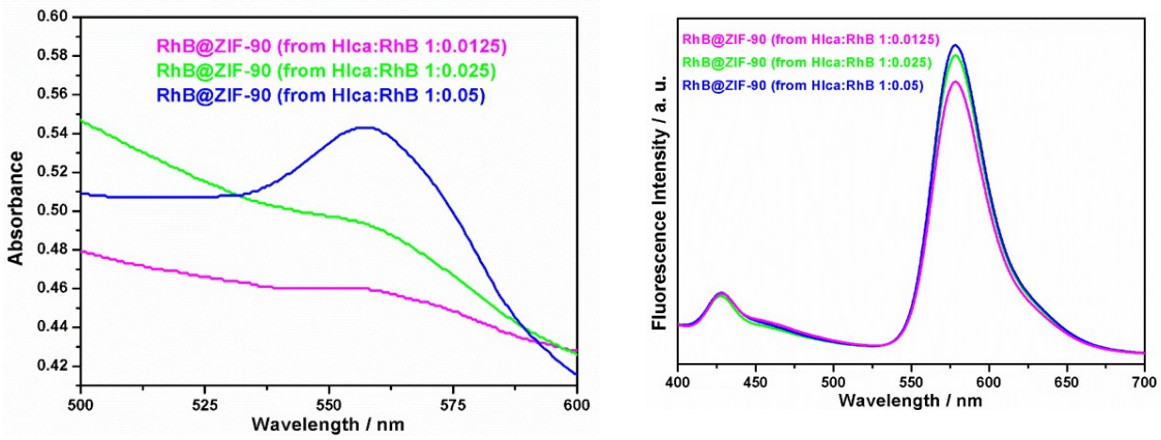

Figure S13. UV-Vis absorption (left) and fluorescence emission (excitation at 373 nm, right) of RhB@NZIF-90 in water prepared from different molar ratios of HIca to RhB.

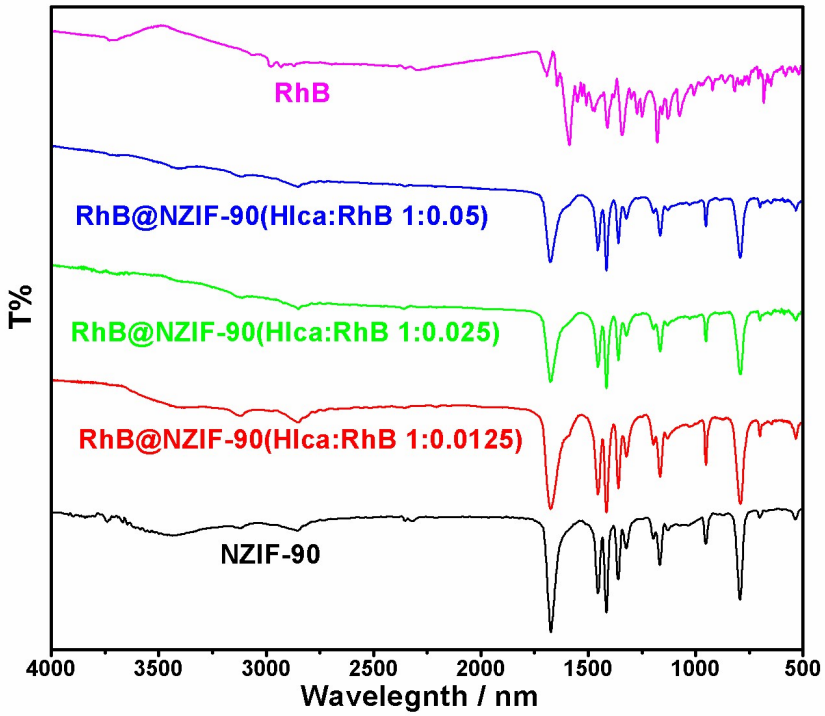

Figure S14. FT-IR spectra of NZI-90, RhB and RhB@NZIF-90 prepared from different molar ratios of HIca to RhB.

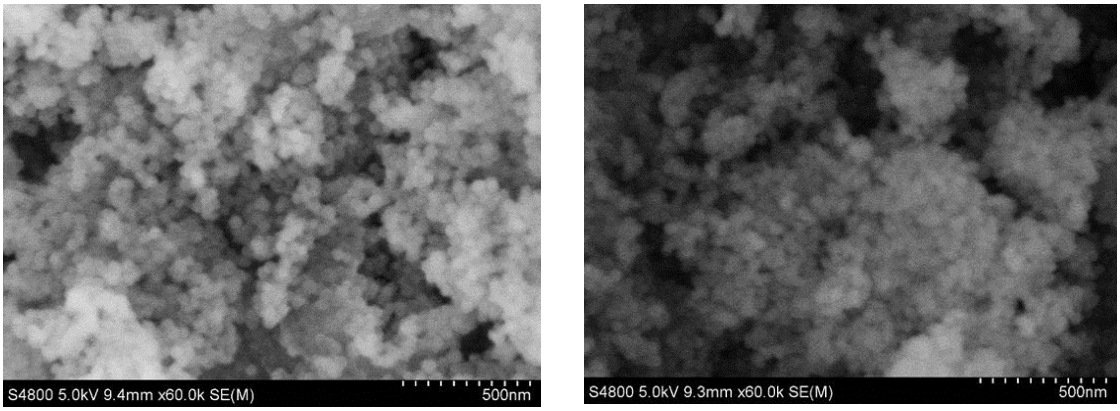

Figure S15. SEM images of RhB@NZIF-90 prepared from different molar ratios of HIca to RhB (1: 0.0125, left; 1:0.025, right).

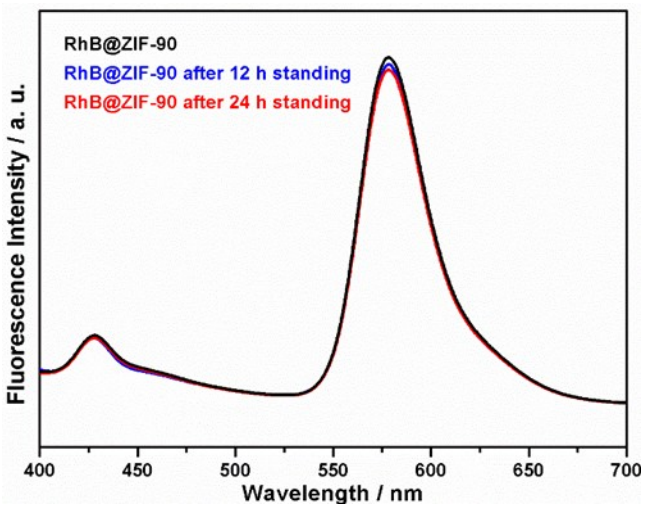

Figure S16. Fluorescence emission spectra of RhB@NZIF-90 in water after 12, 24 h standing.

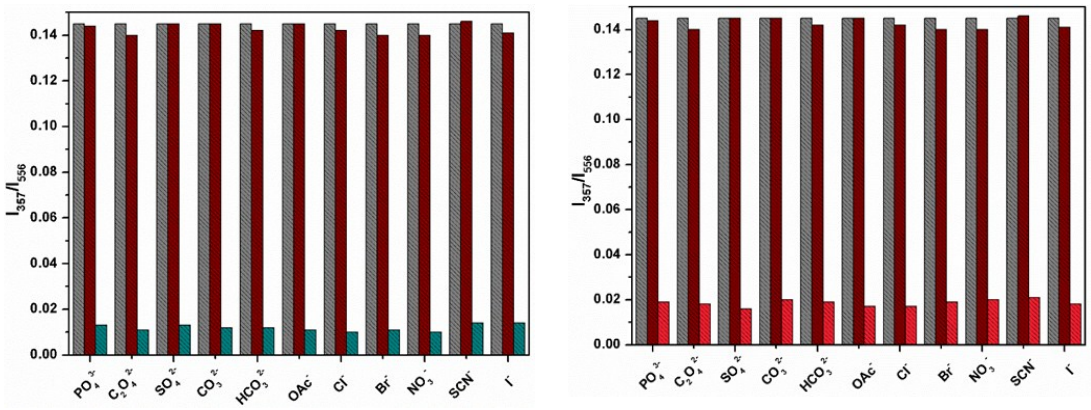

Figure S17. Fluorescence excitation responses of RhB@NZIF-90 (gray bars) to different anions (480 μM, wine bars) and changes in the excitation with subsequent addition of equivalent amount (480 μM) of CrO_4^{2-} (dark cyan bars) and $Cr_2O_7^{2-}$ (pink bars) anions.

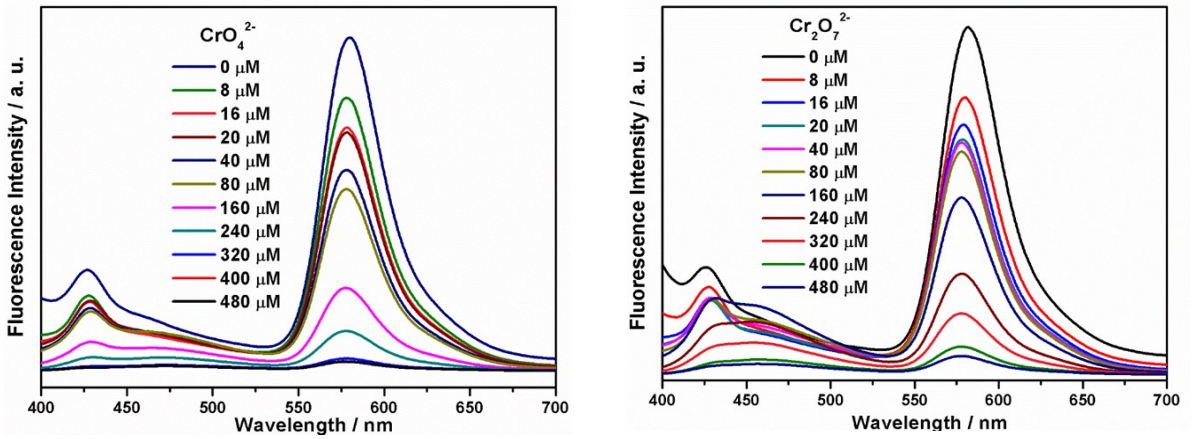

Figure 18. Fluorescence spectroscopic titration of RhB@NZIF-90 water suspension with gradual addition of CrO_4^{2-} and $Cr_2O_7^{2-}$ anions.

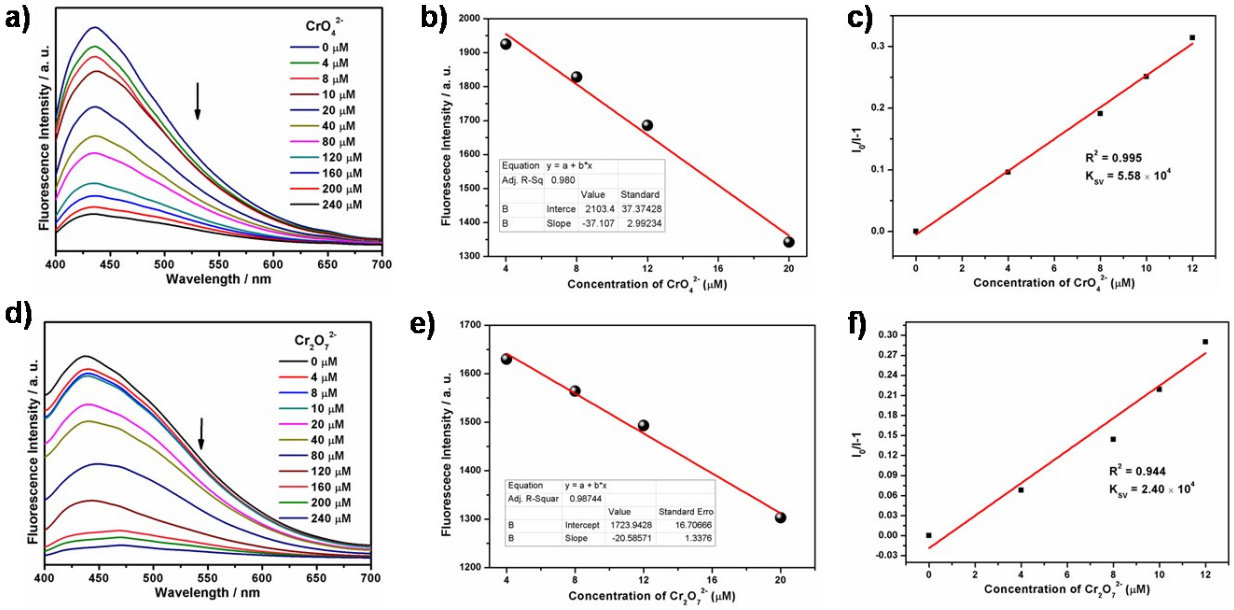

Figure 19. Concentration-dependent fluorescence quenching of NZIF-90 dispersed in ethanol (1.3×10^{-3} M) for CrO_4^{2-} (a) and $Cr_2O_7^{2-}$ (b) anions upon excitation at 373 nm; Fluorescence intensity versus concentration of CrO_4^{2-} (a) and $Cr_2O_7^{2-}$ (b) anions at low concentration range; Stern-Volmer plots of NZIF-90 for CrO_4^{2-} (c) and $Cr_2O_7^{2-}$ (d) anions at low concentration range. The detection limit and quenching constant of NZIF-90 for CrO_4^{2-}/$Cr_2O_7^{2-}$ in ethanol are 1.97 μM and 5.58×10^4 M^{-1}/4.43 μM and 2.49×10^4 M^{-1}.

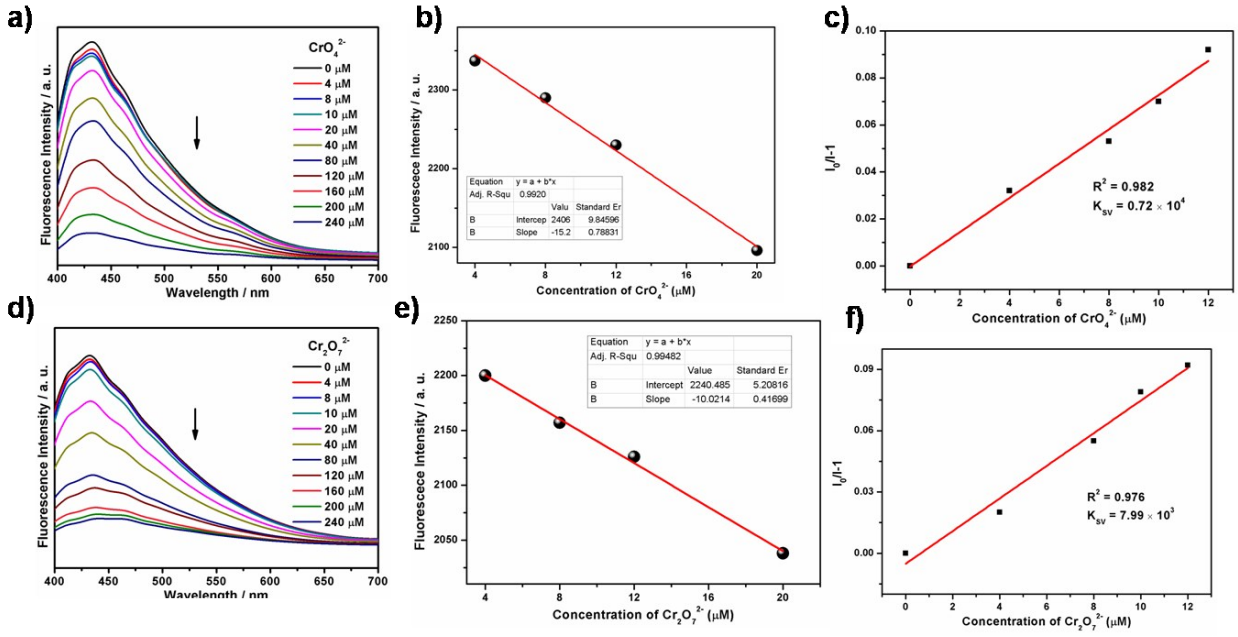

Figure 20. Concentration-dependent fluorescence quenching of NZIF-90 dispersed in DMF (1.3 × 10^{-3} M) for CrO_4^{2-} (a) and $Cr_2O_7^{2-}$ (b) anions upon excitation at 373 nm; Fluorescence intensity versus concentration of CrO_4^{2-} (a) and $Cr_2O_7^{2-}$ (b) anions at low concentration range; Stern-Volmer plots of NZIF-90 for CrO_4^{2-} (c) and $Cr_2O_7^{2-}$ (d) anions at low concentration range. The detection limit and quenching constant of NZIF-90 for CrO_4^{2-}/$Cr_2O_7^{2-}$ in DMF are 3.08 μM and 0.72 × 10^4 M^{-1}/4.68 μM and 0.80 × 10^4 M^{-1}.

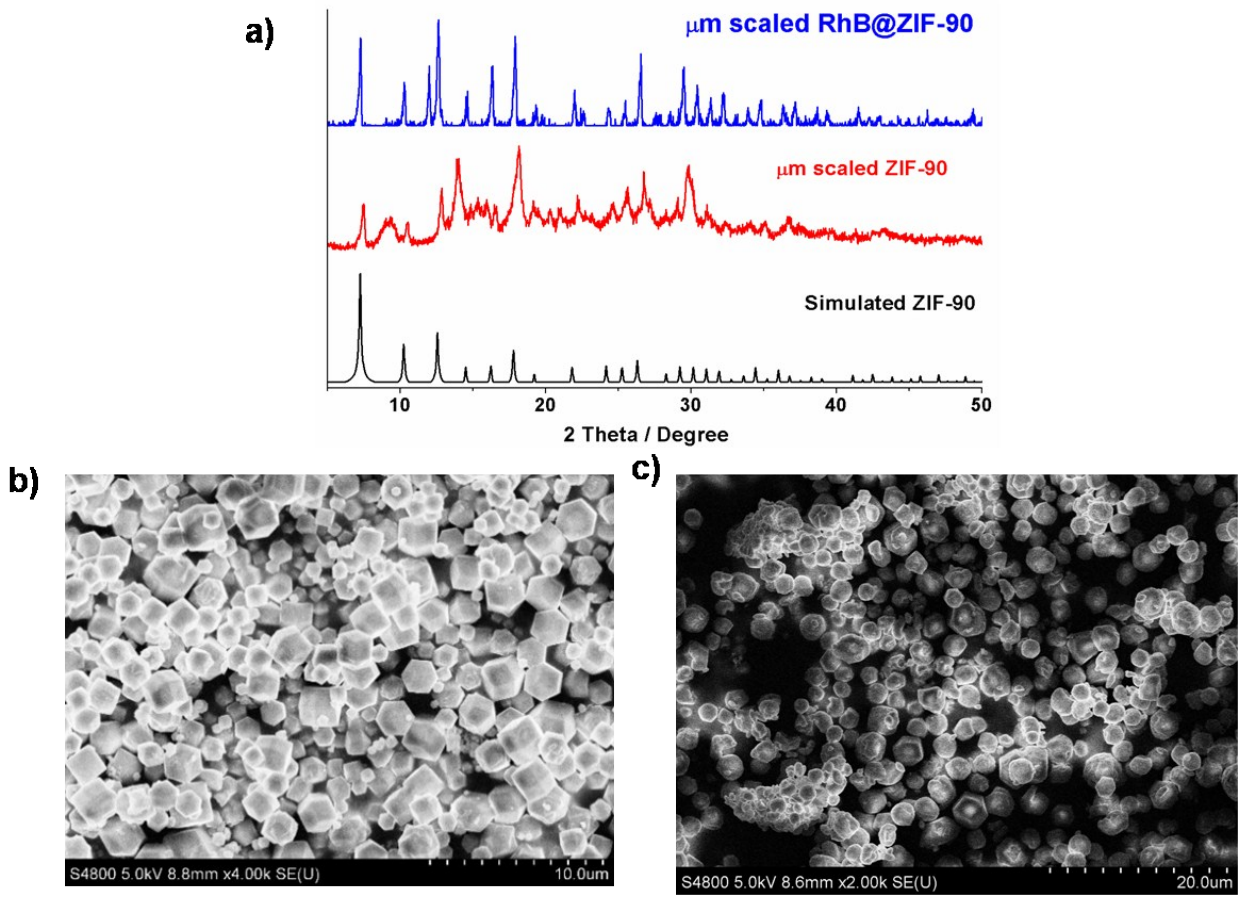

Figure 21. (a) PXRD patterns of the simulated ZIF-90 (black curve), and as-synthesized μm scaled ZIF-90 (red curve) and RhB@ZIF-90 (blue curve); SEM images of the as-synthesized μm scaled ZIF-90 (b) and RhB@ZIF-90 (c).

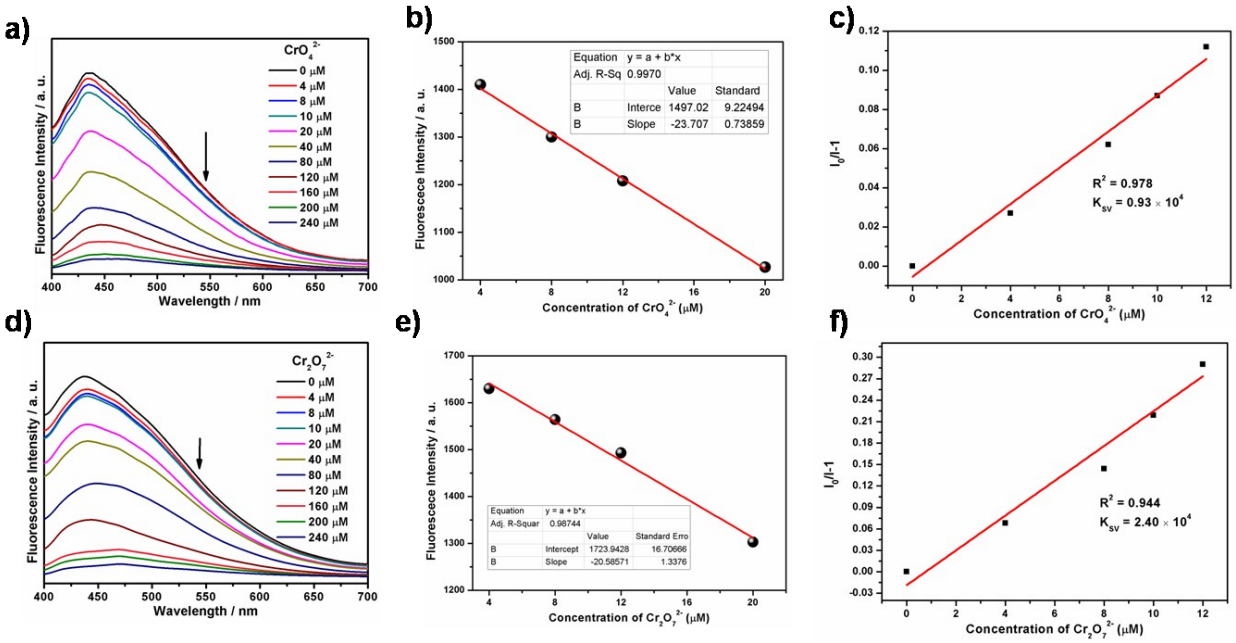

Figure 22. Concentration-dependent fluorescence quenching of μm scaled ZIF-90 dispersed in H_2O (1.3×10^{-3} M) for CrO_4^{2-} (a) and $Cr_2O_7^{2-}$ (b) anions upon excitation at 373 nm; Fluorescence intensity versus concentration of CrO_4^{2-} (a) and $Cr_2O_7^{2-}$ (b) anions at low concentration range; Stern-Volmer plots of NZIF-90 for CrO_4^{2-} (c) and $Cr_2O_7^{2-}$ (d) anions at low concentration range. The detection limit and quenching constant of μm scaled ZIF-90 for $CrO_4^{2-}/Cr_2O_7^{2-}$ in H_2O are 3.76 μM and 0.93×10^4 M^{-1}/4.34 μM and 2.40×10^4 M^{-1}. The μm scaled ZIF-90 was synthesized by increasing the stirring time to 0.5 h as the condition for NZIF-90. The μm scaled RhB@ZIF-90 was prepared according to ref. *J. Am. Chem. Soc.* 2017, 139, 5877-5882.

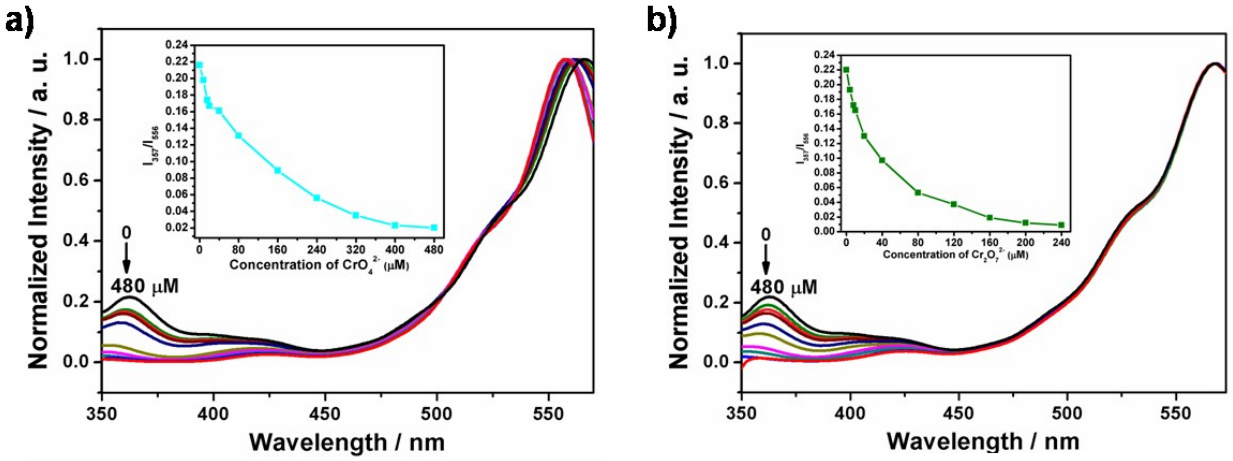

Figure 23. Fluorescence excitation spectral changes of μm scaled RhB@NZIF-90 in the addition of CrO_4^{2-} (a) and $Cr_2O_7^{2-}$ (b) monitored at 582 nm. The insets show the ratiometric response (I_{357}/I_{556}) to varied concentrations of $CrO_4^{2-}/Cr_2O_7^{2-}$ (0 to 480 μM) monitored at 582 nm.